Aerodynamic drag characteristics and shape design of a radar antenna used for airport ground traffic control

Baris Gumusel

Turbomachinery Aero-Heat Transfer Laboratory,
The Pennsylvania State University,
51A Hammond Building, University Park, PA 16802, USA
E-mail: bxg198@psu.edu

Cengiz Camci*

Turbomachinery Aero-Heat Transfer Laboratory,
The Pennsylvania State University,
223 Hammond Building, University Park, PA 16802, USA
E-mail: cxc11@psu.edu
*Corresponding author

Abstract: Modern air traffic control systems in airports use high-speed ground tracking radars usually rotating at 60 rpm. The flow induced vibration and noise generation of the newly developed radar antennas are the two serious problems that jeopardise the successful deployment of the ground aircraft tracking systems. The present study is an attempt to understand the viscous flow characteristics around a typical radar antenna cross section via computations. After a steady-state validation of the computations, a parametric study of possible new shape designs for the antenna is discussed. Significant aerodynamic drag reductions via careful shape design of the antenna are possible.

Keywords: ASDE-X antenna; CFD; computational fluid dynamics; flow visualisations.

Biographical notes: B. Gumusel received a BSc Degree and a MSc Degree in Mechanical Engineering from Istanbul Technical University. He is currently a doctoral candidate in the Department of Aerospace Engineering at the Pennsylvania State University. His current research interests include flow and heat transfer in Turbomachinery.

C. Camci is currently a Professor of Aerospace Engineering at the Pennsylvania State University. He obtained his doctoral degree from the von Karman Institute for Fluid Dynamics in Belgium in 1985. He directed research in the Turbomachinery Aero-heat Transfer Laboratory at Penn State since 1986. He teaches theory of turbomachinery, fluid dynamics, turbulent flow, aerospace propulsion, propulsion systems for un-inhabited air vehicles and finite element methods in fluid dynamics and heat transfer. He is a fellow of the ASME, American Society of Mechanical Engineers.

1   Introduction

More recent "*Airport Surface Detection Equipment*" (ASDE-X) using radar technology requires that the antennas rotate at a minimum speed of 60 rpm.

This recently imposed rotational speed comes from the fact that the ground traffic in a modern airport is tracked and updated once every minute.

The current paper summarises the findings of a Computational Fluid Dynamics (CFD) study performed for the improvement of ASDE-X antenna operation.

The vibration and noise generation of the newly developed ASDE-X radar antenna as shown in Figure 1 is a serious problem that jeopardises the successful deployment of this new airport ground traffic control system. The most significant problem areas are aerodynamically induced noise and vibration. The overall project has three main areas of investigation.

- Experimental wind tunnel research of aero-acoustic/structural characteristics of a scaled rotating antenna model.

- Analytical and numerical studies of aero acoustic.

- CFD studies of the current ASDE-X cross-section and other possible geometries.

Figure 1 The rotating antenna ASDE-X used for airport ground traffic control
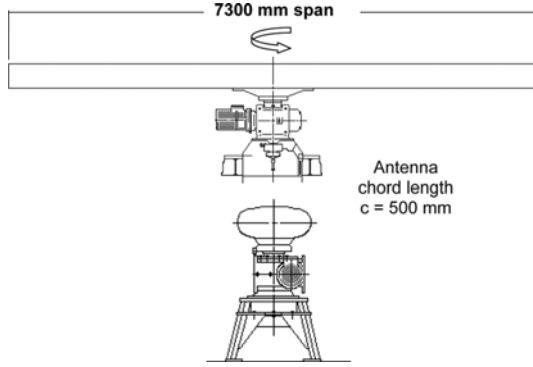
A CFD approach for an accurate assessment of the aerodynamic drag coefficient is used. Proper grid clustering near the wall in the viscous sub-layer is essential in obtaining accurate aerodynamic results. The fluid dynamics details of the re-circulatory flow zones and wakes are simulated at high resolution. The current computational methodology is validated using well-established wind tunnel data for cylinder-in-cross-flow from Prandtl and Tietjens (1934) and Wieselsberger (1914). Additional experimental results are also presented in Flachsbart (1927, 1932) and Roshko (1970). Other '*validation quality*' wind tunnel studies on cylinder in cross flow are reported in Homann (1936), Jones et al. (1969), Schlichting (1979), Blevins (1984) and Hoerner (1965). After the establishment of the validity of cylinder-in-cross-flow computations against wind tunnel data, the actual ASDE-X antenna cross-section shown in Figure 2 is computationally evaluated. In addition, two elongated ellipses are compared against the actual ASDE-X antenna shape and the cylinder.

Figure 2 Structural details of the rotating antenna head and the overall aerodynamic shape
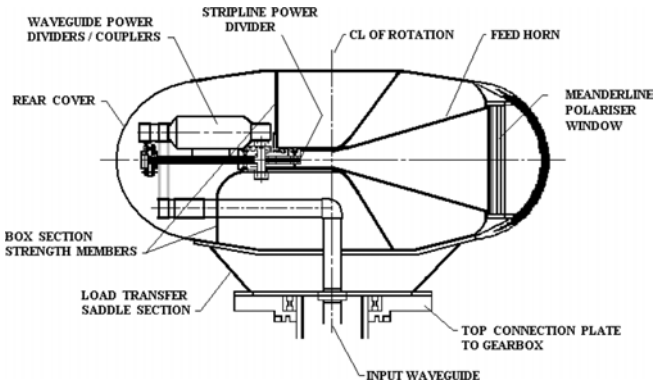
If one replaces the ASDE-X cross section with a cylinder (having the same antenna maximum thickness $H = 0.272$ m) the aerodynamic drag coefficient increases about 60%

relative to the ASDE-X antenna. When the ASDE-X antenna is replaced with an 'equivalent ellipse' having the same Fineness Ratio $FR = c/H$, the aerodynamic drag coefficient is reduced about 19% relative to the original ASDE-X cross-section.

The drag coefficient of the ASDE-X cross section could be reduced about 40% of its original value by simply elongating the ellipse shape to a fineness ratio of $FR = c/H = 2.757$ from the original ASDE-X FR value of 1.838. The elongated ellipse for this case has the new chord length of 1.5 times the original ASDE-X chord. Further elongation of the ellipse to fineness ratios of $FR = 3.5$ and 4.5 seems to provide significant relative improvements.

The drag coefficient in this study was not measured for the specific antenna cross section. The general strategy in this paper is that the computational tool is carefully calibrated/validated for a cylinder in cross flow case using a high quality wind tunnel data set. After validations, the antenna cross sections were evaluated with the validated CFD tool.

2 Governing equations

The numerical simulations of the steady-state 2D flow around the ASDE-X antenna cross section are obtained by solving the incompressible Reynolds Averaged Navier-Stokes equations. The simulations were obtained using the computer code Fluent 6.2 on high quality viscous flow grids. The computational grid systems used is a multi-block structured grid. A two-equation turbulence model based on k-epsilon RNG Re-normalisation Group model was used in all calculations (Yakhot and Orszag, 1986). The near wall treatment was applied without using conventional wall functions. The momentum equations were integrated down to $y^+ = 1$. This approach places a strong emphasis on the quality of the near wall grid system, because of the strong interest in the prediction the drag coefficient of the antenna cross-section. The continuity equation and momentum equations in this model are:

$$U_{i,i} = 0 \tag{1}$$

$$\rho U_j \frac{\partial U_i}{\partial x_j} = -\frac{\partial p}{\partial x_i} + \mu \frac{\partial^2 U_i}{\partial x_j \partial x_j} + \frac{\partial R_{ij}}{\partial x_j} \tag{2}$$

where $R_{ij} = -\rho \overline{u_i u_j}$ are the Reynolds stresses. The Reynolds stresses are modelled by using the Boussinesq hypothesis.

$$R_{ij} = -\rho \overline{u_i u_j} = -\rho \frac{2}{3} k \delta_{ij} + \mu_t \left(\frac{\partial U_i}{\partial x_j} + \frac{\partial U_j}{\partial x_i} \right). \tag{3}$$

For two-equation models, the turbulent viscosity is related to turbulent kinetic energy $k = \overline{u_i u_i}/2$ and the dissipation rate ε as $\mu_t = \rho C_\mu k^2 / \varepsilon$. The turbulent kinetic energy equation is as follows,

$$\rho U_i \frac{\partial k}{\partial x_i} = \mu_t \left[\frac{\partial U_j}{\partial x_i} + \frac{\partial U_i}{\partial x_j} \right] \frac{\partial U_j}{\partial x_i} +$$

$$+ \frac{\partial}{\partial x_i} \left[(\mu + \mu_t / \sigma_k) \frac{\partial k}{\partial x_i} \right] - \rho\varepsilon. \qquad (4)$$

The dissipation rate equation is,

$$\rho U_i \frac{\partial \varepsilon}{\partial x_i} = C_{1\varepsilon} \frac{\varepsilon}{k} \mu_t \left[\frac{\partial U_j}{\partial x_i} + \frac{\partial U_i}{\partial x_j} \right] \frac{\partial U_j}{\partial x_j} - C_{2\varepsilon} \frac{\varepsilon^2}{k} +$$

$$+ \frac{\partial}{\partial x_i} \left[(\mu + \mu_t / \sigma_\varepsilon) \frac{\partial \varepsilon}{\partial x_i} \right] \qquad (5)$$

where $\sigma_k = 1, \sigma_\varepsilon = 1.3, C_{1\varepsilon} = 1.44, C_{2\varepsilon} = 1.92$ are empirical constants.

3   Boundary conditions

Most of the initial calculations were performed for the full-scale ASDE-X tip cross section. A 60 rpm antenna rotational speed was applied. The tip section of the antenna has a linear speed of $U_{tip} = 22.9$ m/s for the tip diameter of $D = 7.3$ m at $N = 60$ RPM. The computational domain is a large rectangular area where the 2D antenna cross-section is located in the central section of the domain as shown in Figures 3 and 4. The left face of the domain was assigned a uniform velocity inlet boundary condition of 22.9 m/s. The top and bottom walls of the computational domain use a zero stress boundary condition in order to eliminate the development of boundary layers and an eventual core flow blockage. The antenna surface uses a no-slip boundary condition. The downstream boundary conditions impose that the streamwise gradients of the mean velocity components are zero at the exit section (outflow condition). A turbulence intensity of $Tu_\infty = 0.5\%$ and a turbulent length scale of $L = 0.25$ m are imposed at the inlet section. These are estimated average values of atmospheric turbulence that might occur around a typical ASDE-X antenna. The air density at standard sea level conditions was taken as $\rho = 1.225$ kg/m^3. The molecular viscosity used in the calculations is $\mu = 1.789 \times 10^{-5}$. The Reynolds number of the tip section is Re $= [\rho U_{tip} H / \mu] = 426,000$ based on $U_{tip} = 22.9$ m/s and $H = 0.272$ m ($H =$ maximum height of the antenna cross section) at 60 RPM. The chord length of the actual ASDE-X cross section is 0.5 m.

Figure 3   2D computational domain 41626 grid point
   (a mix of block structured and unstructured grid)
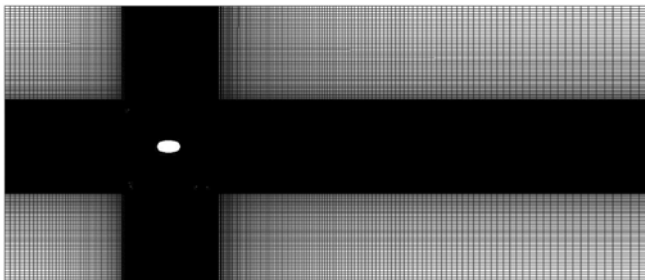
Figure 4   Grid system near the antenna and the boundary
                layer grid used in drag coefficient calculations
   *c/H = Fineness ratio*
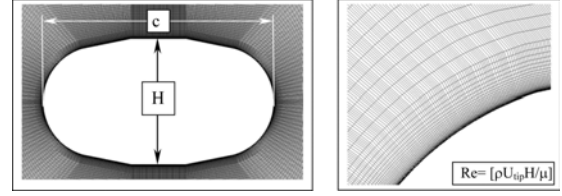
4   Mesh dependency

Mesh design is an important part of CFD study. Incorrect definition of a mesh will result in unrealistic solution data. In this study, a comprehensive mesh dependency test was performed on a cylinder and antenna geometry. The drag coefficient value was calculated for a gradually refined series of meshes. Starting from a node number of approximately 300 nodes around a cylinder and antenna, the grid point around the body was progressively refined testing approximately 500, 600, 800, 1000, 1200, 1400 and 1700 node points. Typical results of the mesh dependency test are shown in Figure 5. Since total cell number increases with increasing number of node points around the body, Figure 6 is also given as typical results of the mesh dependency test. The percentage difference in drag coefficient value between the mesh with 300 node points and the finest mesh was $(0.29 - 0.21)/0.29 = 28\%$.

Figure 5   Mesh dependency test with respect to grid points
                around a cylinder and antenna
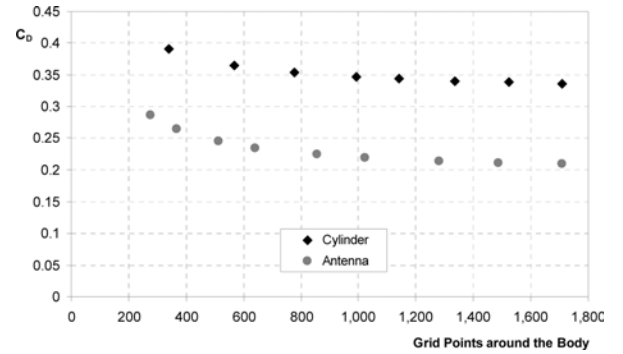
Figure 6   Mesh dependency test with respect to total grid points
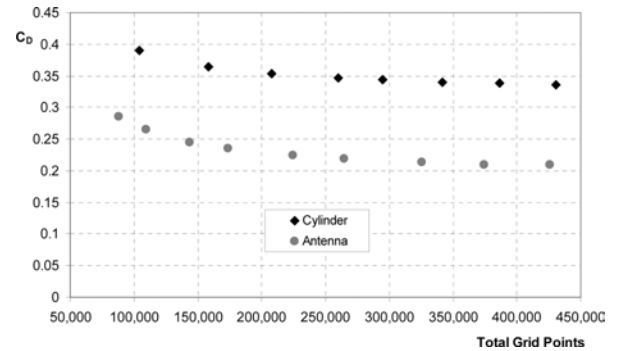

Based on the results, the finest mesh was used for the simulations.

5 Validation of the computations

5.1 Validations for a cylinder in cross flow

The accuracy of drag coefficient computations were checked by using a well established experimental data set from Wieselsberger (1914) as published by (Prandtl and Tietjens, 1934) and (Schlichting, 1979). Figure 7 shows the variation of drag coefficient C_D with respect to Re $= \rho U_{tip} H/\mu$ for a circular cylinder of infinite aspect ratio and finite length to diameter ratio of 5 : 1. The C_D data set was obtained by systematically increasing cylinder diameters so that the Reynolds numbers above 10^4 are covered.

Figure 7 C_D with respect to Re $= \rho U_{tip}H/\mu$ for a circular cylinder of infinite aspect ratio and finite length to diameter ratio of 5 : 1
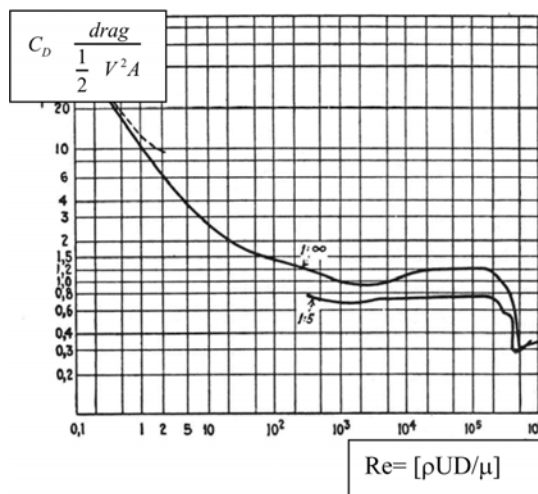
Source: Prandtl and Tietjens (1934), Wieselsberger (1914) and Roshko (1970)

The measured data set shows a transition to supercritical operation at Re = 400,000. The values before Re = 200,000 are usually termed as '*laminar*' in the literature. Below Re = 200,000, the onset of separation point is on the frontal part of the cylinder near 90° point. The drag coefficient remains constant at a value around $C_D = 1.2$ in a wide Reynolds number range from Re = 1000 to 200,000. Increasing Re in this wide range does increase the drag force; however the increase in the denominator of the drag equation (Dynamic head × Frontal area) results in a constant drag coefficient. After Re = 200,000, the onset of separation point near the 90° point moves to the aft part of the cylinder all of a sudden. Any small increase in this range results in further closing of the wake region around the cylinder. The overall wake dimension in cross-stream direction becomes smaller and smaller with increasing Reynolds number. The C_D values continually decline up to Re = 450,000. The inset in the lower figure shows C_D variation this special region. The drag coefficient slightly increases between Re = 450,000 and 1,000,000. The pressure drag in this range is likely to increase faster.

The current validation of the computations was performed at the actual tip $Re_{tip} = 426,000$ of the ASDE-X antenna. Drag coefficient of a circular cylinder at this specific Reynolds number was computationally investigated. The current computations predict a cylinder drag coefficient of $C_D = 0.3363$. This computationally predicted value is in very good agreement with the measured drag coefficients as shown in Figure 8.

Figure 8 Wieselsberger's (1914) cylinder in cross flow measurements from Prandtl (1934). The red plus symbol is the present computational prediction of $C_D = 0.3363$ at Re = 426,000 (see online version for colours)
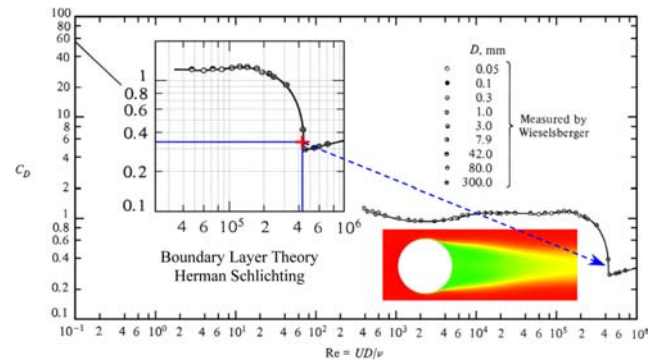

Figure 8 is usually used as a summary of Wieselsberger's experiments for Re > 10,000. Ellipse in cross flow experimental data is also provided for various fineness ratios (*FR* = *c*/*H*) in Figure 9. The term laminar is used for the Re range before the discontinuity around Re = 200,000, where the term 'turbulent' is used for the range after Re = 450,000. The current computational predictions for the cylinder and ellipse are also in good agreement with the summary table given in Yakhot and Orszag (1986). A second validation computation for an ellipse of *FR* = 1.83 was performed. The predicted C_D value for this ellipse was 0.1699. This value compares well with the measured C_D value of 0.20 (*FR* = 2) from Figure 9.

Figure 9 A summary of measured drag coefficients for Re > 10,000 for a circular cylinder and ellipses of various fineness ratios (*FR* = *c*/*H*)
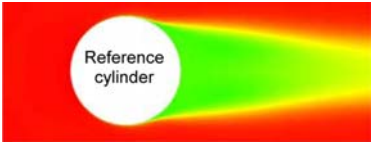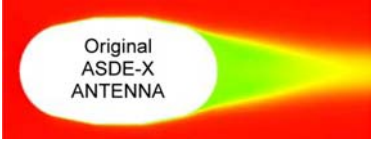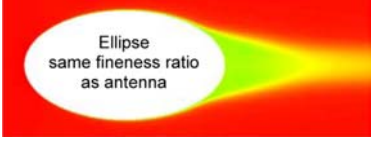

Source: White (2002)

## 6	Computational results and discussion

This section presents results for the drag coefficient of a reference cylinder having the same frontal area of the ASDE-X antenna, the actual antenna geometry and two other suggested cross sections for the future antenna designs. The drag coefficient in this investigation is defined as C_D = drag/$(0.5\ \rho V^2 A)$ where 'drag' includes both pressure drag and viscous drag forces. A is the frontal area of the antenna cross section which is defined as $A = [H \times$ Antenna length] where H is the maximum thickness of the ASDE-X cross-section or the diameter of the reference cylinder. Antenna length is unity for 2D calculations. The 2D solid contours shown in Tables 1, 3 and 4 show the distribution of total pressure as an indication of local momentum deficit in the boundary layer and wake. Red is the highest total pressure and green is the lowest level of total pressure.

### 6.1	Different geometries with the same frontal area

Table 1 compares the computed drag coefficients for the ASDE-X tip cross section, a reference cylinder, and two ellipses having the same effective cross section. The viscous force in horizontal direction, the pressure force and the total horizontal force is presented. The horizontal force components are calculated by integrating the wall shear stress and pressure over the aerodynamic shapes. The highest drag value is assigned to the cylindrical cross section due to a relatively early onset of separation point near the 90° location. Moving from the cylinder to ASDE-X cross section, presents a 38% improvement in the drag coefficient. Table 1 shows that an ellipse of the same fineness ratio as the ASDE-X antenna can improve the drag coefficient by about $RI = 19\%$.

Table 1	A comparison of the computed ASDE-X antenna aerodynamics with a cylinder and two ellipses $H = 0.272$ m, $c = FR \times H$, Re = 426,000 (see online version for colours)
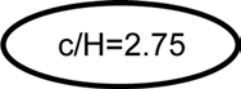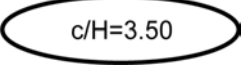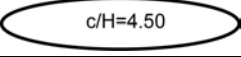
Objects	Pressure force (N)	Viscous force (N)	Total force 'drag' (N)	Drag coefficient C_D	Fineness ratio $FR = c/H$
Reference cylinder	27.95	1.44	29.39	$C_D = 0.3363$	1.000
Original ASDE-X ANTENNA	16.07	2.24	18.31	$C_D = 0.2096$ $RI = 0\%$	1.8382
Ellipse same fineness ratio as antenna	12.52	2.32	14.84	$C_D = 0.1699$ $RI = +19\%$	1.8382
Elongated ellipse	8.29	2.98	11.27	$C_D = 0.1291$ $RI = +38\%$	2.7574

When the ellipse is elongated further to $FR = c/H = 2.75$, a significant C_D gain in the order of RI = 38% is obtained when compared to the ASDE-X cross section. The '*relative improvement RI*' is defined as the ratio of '*the drag coefficient reduction*' divided by the "*drag coefficient of ASDE-X cross section*". In elliptical cross sections, the wake thickness and the momentum deficit is effectively reduced.

The influence of increasing the fineness ratio of an elliptical cross section at the tip Reynolds number level is presented in Figure 9. An ellipse of $FR = 2.75$ results in a C_D of 0.1291. This relative improvement level is equivalent to about $RI = 38\%$ of the ASDE-X cross section C_D value. Increasing the fineness ratio from $FR = 2.75$ to 3.5 only results in a relative improvement in aerodynamic performance $(RI = 44\%)$. The highest fineness ratio of $FR = 4.5$ results a C_D of 0.1112 with a relative improvement value of $RI = 47\%$. Table 1 clearly show that the most dramatic improvement in using elliptic antenna shapes can be obtained when the ASDE-X cross section is replaced with an ellipse of equivalent $FR = 1.838$ and 2.757. Although further elongation of the antenna shape brings improved drag coefficients, the operation of the extremely flat elliptical shape with an increased chord length may prove difficult from fluid-solid interaction point of view. Table 2 shows additional computational results from $FR = 3.5$ and 4.5 ellipses. Extremely flat elliptical shapes may also result in radar antenna integration problems in the rotating cross section.

Table 2 A comparison of three elliptical cross sections with different fineness ratios $H = 0.272$ m, $c = FR \times H$, Re = 426,000 (see online version for colours)
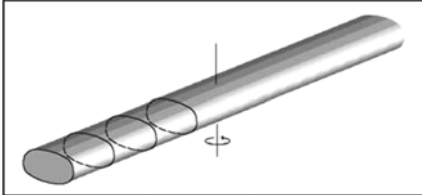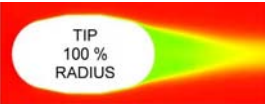
Objects	Pressure force (N)	Viscous force (N)	Total force (N)	Drag coefficient C_D	Fineness ratio $FR = c/H$
c/H=2.75	8.29	2.98	11.27	0. 1291 $RI = 38\%$	2.7574
c/H=3.50	6.79	3.45	10.24	0. 1172 $RI = 44\%$	3.5
c/H=4.50	5.68	4.04	9.72	0. 1112 $RI = 47\%$	4.5

6.2 Cross sections between the antenna hub and tip

Table 3 shows the computed drag coefficients for the ASDE-X cross-section at four different radial positions from the tip to hub (25% radius). Since the antenna is rotating at 60 RPM, the linear velocity of the sections at 100%, 75%, 50% and 25% tip radius result in different Reynolds numbers. The four radial sections are indicated in the solid model of the antenna in Table 3.

Table 3 Aerodynamic performance of the ASDE-X antenna at four radial positions from tip to hub (see online version for colours)

Objects	Pressure force (N)	Viscous force (N)	Total force (N)	Drag coefficient C_D	Fineness ratio $FR = c/H$
TIP 100 % RADIUS	16.07	2.24	18.31	0.2096	1.8382
75 %	9.05	1.34	10.39	0.2108	1.8382
50 %	4.09	0.65	4.74	0.2152	1.8382
HUB 25 % RADIUS	1.05	0.18	1.23	0.2250	1.8382

The drag coefficients slightly increase from 0.2096 to 0.2250 from tip to hub because of the decrease in Reynolds number assigned to each section at 60 RPM. The total increase is within 7.3% of the tip value of C_D. The total pressure values in each section and the horizontal total force (viscous + pressure) are reduced significantly from tip to hub. The 25% radius section near the hub experiences 15 times less total force when compared to the tip section, due to important reductions in the dynamic head assigned to this cross section. The ratio of the viscous force to pressure force in each section remains approximately constant at about 15%.

6.3 Comparison between the full scale and small scale computations

The aerodynamic performance of the scale wind tunnel antenna used in this study was compared to the full scale ASDE-X antenna cross section at the tip section. The only computational difference in the two cases is in the Reynolds number assigned to each cross section. The actual antenna rotating at 60 rpm had a tip speed of 22.9 m corresponding to a tip Reynolds number of 426,000. 1/10 scale antenna used in the wind tunnel studies was rotated at 600 RPM so that the tip speed of the wind tunnel model matches the

tip speed of the actual ASDE-X antenna. The computational results for the full scale operation are given in the top row of Table 4. The wind tunnel model tip Reynolds number was ten times smaller compared to the actual ASDE-X antenna. The lower row of Table 4 is for the 1/10 scaled model operating at Re = 42,600 (*H* = 0.0272 m), 600 RPM.

The predicted drag coefficient for the 1/10 scale wind tunnel model is $C_D = 0.2663$. The relative increase in the drag coefficient is about 27% with respect to full scale operation. Although the change in Reynolds number is ten fold, a slight change in the computed drag coefficient was observed. This weak Reynolds number dependency of computations is consistent with measured trends.

Table 4   A comparison of the full scale ASDE-X antenna and the 1/10 scale PSU wind tunnel model, *c*/*H* = 1.8382 (see online version for colours)

Objects	Pressure force (N)	Viscous force (N)	Total force (N)	Drag coefficient C_D	Fineness ratio FR = c/H
FULL SCALE	16.07	2.24	18.31	0.2096	1.8382
1/10 SCALE	1.98	0.35	2.33	0.2663	1.8382

Figure 10 shows the influence of aerodynamic shape design on the static pressure distribution around the reference cylinder, actual ASDE-X antenna and two elongated ellipses. The static pressure disturbances generated by the sharp corners of the original ASDE-X antenna are clearly visible in Figure 10. Figure 11 presents the numerical simulation of the streamlines in the re-circulatory flow zone of the four aerodynamic objects. A clear reduction in the size and momentum deficit of the wakes from ellipses is noticeable. A reduced wake size and momentum deficit is expected to reduce the severity of the wake-antenna interactions. The interactions may be strong especially when cross-winds exist around the rotating antenna assembly. This is the case where the antenna may be chopping its own wakes due to highly three dimensional wind loads.

Figure 10   Static pressure field around the cylinder, antenna and two ellipse cross sections (in N/m^2) (see online version for colours)
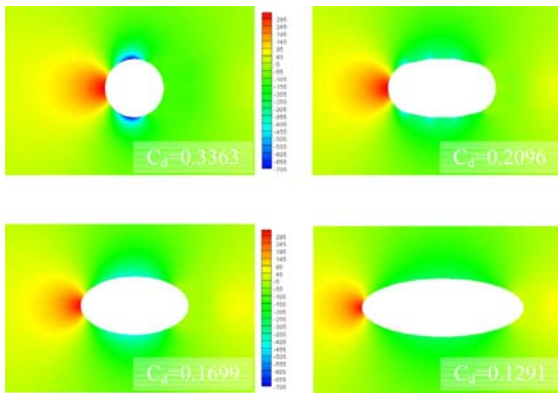
Figure 11   Wake re-circulatory flow structure around the cylinder, antenna and two ellipse cross sections (see online version for colours)
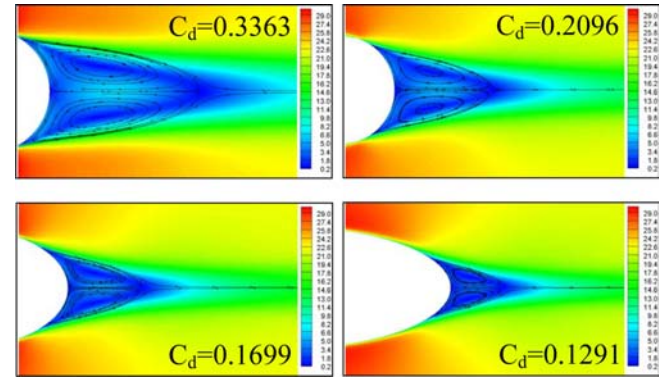
7   Conclusions

The results from a 'CFD' study around an ASDE-X antenna are used to understand viscous flow details and vortex shedding characteristics under 'full scale' and 'scaled model' operating conditions.

The computational method using a two-equation (K-Epsilon RNG) turbulence model with a near wall grid addressing the need for the discretisation of the viscous-sub layer are the two key elements in predicting pressure drag and viscous drag.

The present computations were validated by using well known experimental data for a cylinder in cross flow case, at the full scale Reynolds number of 426,000. The predicted drag coefficient for the cylinder agrees very well with the measured C_D values.

If one replaces the ASDE-X cross section with a cylinder (having the same antenna maximum thickness H) the aerodynamic drag coefficient increases about 60% relative to the ASDE-X antenna. Although it may not be possible to house an antenna in a cylindrical geometry, this case was studied, as a reference shape for which there is extensive experimental fluid mechanics data.

If the ASDE-X antenna is replaced with an equivalent ellipse: having the same fineness ratio, the aerodynamic drag coefficient could be reduced by about 19% relative to the original ASDE-X cross section.

The drag coefficient of the ASDE-X cross section could further be reduced by about 38% relative to the original value by simply elongating the ellipse shape to a fineness ratio of $FR = c/H = 2.757$ from the original ASDE-X FR value of 1.838. The elongated ellipse for this case has the new chord length of 1.5 times the original ASDE-X chord.

Further elongation of the ellipse to fineness ratios of $FR = 3.5$ and 4.5 seems to provide relative improvements of $RI = 44\%$ and $RI = 47\%$, respectively. Although a relative improvement in C_D is observed, due to increased antenna perimeter, these flattened shapes may be very sensitive to varying external aerodynamic conditions in terms of fluid-solid interaction characteristics.

The drag coefficients slightly increase from a tip value of $C_D = 0.2096$ to 0.2250 at the 25% antenna radius (hub). Due to a monotonic reduction in linear speed at each radial position, the horizontal aerodynamic force (pressure + viscous force) is about 15 times smaller at the hub (25% radius) than the tip value. This prediction suggests that fluid solid interactions near the tip section are much more significant in the last quarter of the antenna radius.

The aerodynamic performance of the scale wind tunnel antenna used in this study was compared to the full scale ASDE-X antenna cross section at the tip section. The predicted drag coefficient for the 1/10 scale wind tunnel model is $C_D = 0.2663$. The relative increase in the drag coefficient is about 27% with respect to full-scale operation. Although the change in Reynolds number is ten fold, a slight change in the computed drag coefficient was observed. This weak Reynolds number dependency of computations is consistent with measured drag coefficients of aerodynamic objects such as cylinders and ellipses.

References

Blevins, R.D. (1984) *Applied Fluid Dynamics Handbook*, Van Nostrand Reinhold, New York, ISBN: 9780442212964, p.558.

Flachsbart, O. (1927) 'Recent researches on the air resistance of spheres (German)', *Physikalische Zeitschrift*, Vol.28, No.13, pp.461–469.

Flachsbart, O. (1932) 'Winddruck auf Gasbehalter', *Reports of the AVA in Gottingen*, IV th Series, Vol. 4, No. 4, pp.134–138.

Hoerner, S.F. (1965) *Fluid-Dynamic Drag: Practical Information on Aerodynamic Drag and Hydrodynamic Resistance*, Self-published work, Library of Congress Card Number 64-19666, Washington, DC, pp.60–166.

Homann, F. (1936) 'Einfluss grosser Zahigkeit Bei Stromung um Zylinder', *Forschung im Ingenieurwesen*, Vol. 7, No. 1, pp.1–10.

Jones, G.W., Cincotta, J.J. and Walker, R.W. (1969) *Aerodynamic Forces on a Stationary and Oscillating Circular Cylinder at High Reynolds Numbers*, Report Number NACA TR-R-300, pp.1–62.

Prandtl, L. and Tietjens, O.J. (1934) *Applied Hydro- and Aeromechanics*, Dover Publications Inc., New York, ISBN: 486-60375-X, p.311.

Roshko, A. (1970) 'Experiments on the flow past a circular cylinder at very high Reynolds numbers', *Journal of Fluid Mechanics*, Vol.10, pp.345–356.

Schlichting, H. (1979) *Boundary Layer Theory*, 7th ed., McGraw-Hill, New York, ISBN: 0070553343, pp.425–428.

White, F. (2002) *Fluid Mechanics*, 5th ed., McGraw-Hill, New York, ISBN: 0072831804, p.866.

Wieselsberger, C. (1914) 'The air resistance of spheres (German)', *Zeitschrift für Flugtechnik und Motorluftschiffahrt*, Vol. 5, pp.140–145.

Yakhot, V. and Orszag, S.A. (1986) 'Re-normalisation group analysis of turbulence', *Journal of Scientific Computing*, Vol. 1, No. 1, pp.3–51.